Project Title:

Theoretical study of interaction between tunneling electrons and individual molecules at surfaces

Name: ○Yousoo Kim, Emi Minamitani, Jaehoon Jung, Hiroshi Imada, Miyabi Imai

Laboratory at RIKEN: Surface and Interface Science Laboratory

1. Background and purpose of the project, relationship of the project with other projects.

During the past decade, computer simulations based on a quantum mechanics have developed an increasingly important impact on solid-state physics and chemistry and on materials science. In field of material science, the surface chemistry is fundamentally important in many areas, such as molecular electronics, heterogeneous catalyst, fuel cell, etc. The adsorption of molecules onto a surface is a necessary prerequisite to any surface mediated chemical process. Understanding the bonding nature between the molecule and the surface on the basis of the electronic structure is therefore one of the most important issues in this field. The computational methods like density functional theory (DFT) have played a prominent role to elucidate the interaction between the molecule and the surface. In addition, the computational method can be useful to study the details of energy transport and conversion among photon and electrons mediated with adsorbate at solid surfaces in the nanoscale regime.

From the theoretical investigation of the adsorbed molecule on surface in combination with scanning tunneling microscopy and spectroscopy (STM/STS) experiment, we could expect the following research goals; 1) the deep understanding of the chemical/physical properties of an adsorbate on the surface not only in ground state but also in excited state, 2) the fine control of the chemistry on the surface.

2. Specific usage status of the system and calculation method

We have been studying the molecular adsorption on the well-defined metal surface using computational method in combination with experimental method. In our studies, first-principles simulations have been carried out using the Vienna Ab-initio Simulation Package (VASP) code in the density functional level of theory. The pure DFT methods have been mostly used and the inner electrons are replaced by projector augmented wave pseudopotentials (PAW). The climbing image nudged elastic band method (CI-NEB) was used to determine the transition states which were confirmed by imaginary frequency modes. In most of cases, STM image simulations were performed using Tersoff-Hamann approach. The computational results have been compared with the available experimental result obtained from STM in our group. For the gas phase molecules, the Gaussian09 program with atomic-orbital basis set was also effectively utilized to obtain stable geometries and corresponding electronic structures.

We also have been studying the many-body phenomena in molecular adsorption system, in particular the Kondo effect. The characteristic electronic state resulting from the Kondo effect, so-called Kondo singlet state appears as a sharp peak structure (Kondo peak) at the Fermi level in STS. In order to simulate the Kondo peak, we build numerical renormalization group (NRG) code and the STS simulation code based on the Keldysh Green's function method.

３．　Results

(1) Dispersive Electronic States of the π‑Orbitals Stacking in Single Molecular Lines on the Si(001)‑(2×1)‑H Surface

Conductive nano-wires are indispensable for realization of the ultimately miniaturized electronic circuits in molecular scale. Together with the recent significant progress in the developments of single molecular devices, e.g., rectifiers, switch junctions, and transistors, a number of challenging studies on the molecular nano-wires have been conducted to gain control over the size, conductivity, and also constructiveness between the single molecular devices on a substrate. As a candidate for the charge transport nano-wires, one-dimensional (1D) molecular assemblies grown through the dangling-bond-initiated chain reactions on the H-terminated Si(001)-(2×1) surface are promising, because not only length and location but also direction of the molecular line growth can be controlled.

In this study, the electronic state characterization of the 1D benzophenone lines on Si(001)‑(2×1)‑H were carried out by the combination of an angle-resolved ultraviolet photoelectron spectroscopy (ARUPS) and periodic density functional theory (DFT) calculations with morphological verification by STM. The theoretically optimized molecular assembly was corroborated in comparison with their high-resolution STM images. The observed peaks in the UPS spectra were reproduced by the calculation, in which the dispersive feature consists of the π-orbitals of stacking Ph rings in the assembled benzophenone. The energy shift in k-space was comparable to that of the organic materials giving the high carrier mobility in the thin film transistors.
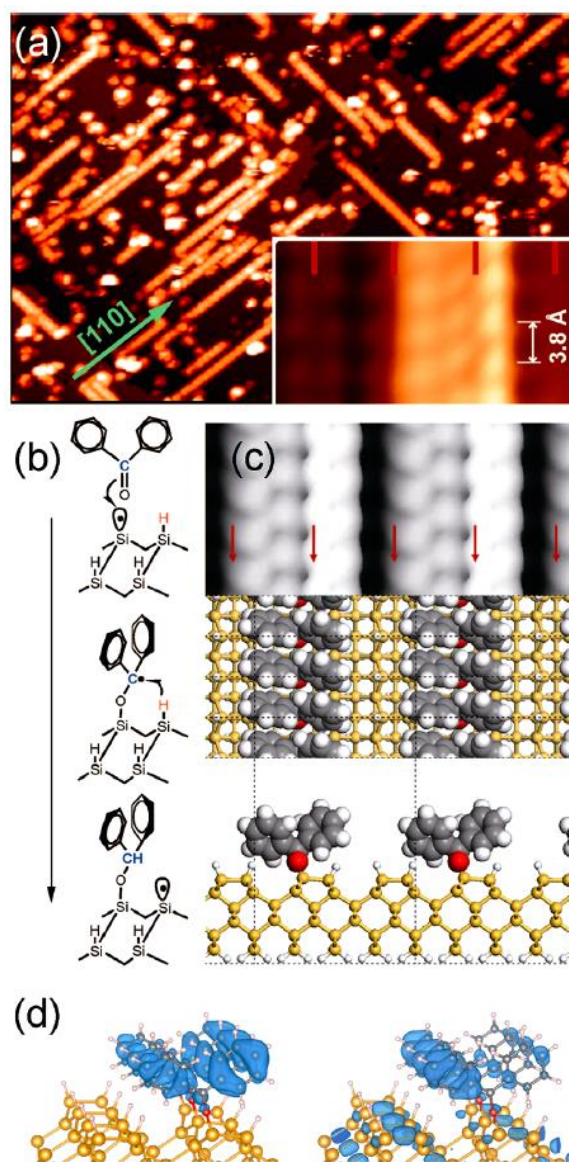

Figure 1. View graphs of benzophenone molecular assemblies on Si(001)-(2×1)-H: (a) a typical STM image (V_s = -2.8 V, I_t = 0.2 nA, 90×62 nm^2) and a zoomed image (inset: V_s = +1.0 V, I_t = 0.2 nA, 2.8×1.5 nm^2); (b) schematic reaction steps; (c) top and side views of calculated benzophenone lines; and (d) calculated orbitals of the benzophenone assembly, with the HOMO at ~1.1 eV in binding energy (left) and the HOMO-1 at ~1.4 eV (right). In the inset of (a), the center positions of the Si dimers are marked by red bars. In (c), the upper panel shows a simulated constant current STM image (V_s = +1.5 V), with red arrows marking the Si dimer center. The unit cell in our calculation is shown by dotted lines in (c).

Fig. 1a shows a typical STM image of benzophenone dosed Si(001)‑(2×1)‑H; various length but equally directed single molecular lines following the Si dimer row direction on each terrace are seen. The self-assembled molecular lines are formed through a chain reaction initiated by dangling bond sites on

Si(001)-(2×1)-H, as shown in Fig. 1b. The >C=O double bond of benzophenone becomes a >CH−O−Si linkage by creation of an O−Si covalent bond at a dangling bond site followed by H-atom abstraction from the nearest-neighbor monohydrated dimer Si to the >C•− radical site. The H abstraction from the nearest-neighbor site, consequently, leads the molecular line to be grown at a side of the Si dimer row, as in the inset of Fig. 1a, in which the center of the molecular lines is off from the center of dimer rows (red bars). Note that the sp^2-type >C= site of the carbonyl group becomes an sp^3-type >CH− site after the H abstraction. Hence, the two Ph rings of the assembled molecule are no longer in a π-conjugate, and the electronic states of the two may not be equivalent. It is fact that the on-dimer side of the benzophenone assembly is slightly brighter than the off-dimer side, as shown in the high resolution STM image (inset of Fig. 1a). Because the molecular periodicity in the assembly is close, that is, the distance between the Si dimers along the row (3.84 Å), the π-orbitals of each Ph ring must stack individually and thus possibly interact along the assembly.

Details of the benzophenone assembly on Si(001)-(2×1)-H were examined using periodic DFT calculations. The optimized geometry of the assembly was corroborated in comparison between the high-resolution STM images and the calculated one based on the Tersoff−Hamann approach. Fig. 1c shows the simulated STM image with the top and side views of the optimized benzophenone assembly, which reproduces well the observed high-resolution STM image. Our computational results revealed that the different electronic structure between two Ph rings is attributed to the symmetry breaking of the isolated benzophenone molecule (C_2 symmetry) at the adsorption; the off-dimer Ph plane becomes nearly perpendicular to the −C−O− linker, while the on-dimer Ph plane still includes the linker. This symmetry breaking results from the change in hybridization of the −C−O− linker group, that is, sp^2 to sp^3, and the asymmetrical environment of the substrate, that is, on-dimer and off-dimer rows, with respect to the positions of Ph rings. Therefore, this geometric difference induces the splitting of π-states of two Ph rings, as shown in Fig. 1d, where the first occupied π-state (~1.1 eV below the Fermi level), that is, the highest occupied molecular orbital (HOMO), is distributed mainly at the on-dimer Ph and the next dominant π-state (~1.4 eV), attributed to HOMO− 1, shows wider distribution on both on- and off-dimer Ph rings with a substrate component due to level alignment between the adsorbate and substrate orbitals.

To elucidate the π-state features of the benzophenone assembly, we measured UPS spectra of them. The UPS spectra are also compared with the calculated results, as shown in Fig. 2a. The spectra (i) and (ii) were measured at the Si(001)-(2x1)-H surface before and after the benzophenone dose, respectively. Their onsets below 2 eV in binding energy overlapped each other, and thus, the three additive intense peaks at 3.5, 6.5, and 8.6 eV on spectrum (ii) were attributed to the signals from the benzophenone assemblies, as previously reported. Spectrum (iii) was obtained from the calculated local density of states (LDOS) of the benzophenone assembly on Si(001)-(2x1)-H at the Γ point in k-space with broadening by the Gaussian function of σ = 0.5 eV. The calculated spectra reproduced the three intense peaks, though the energy levels and relative intensity ratio of the peaks were somewhat incomplete. The energy level shift by a few eV is due to a weakness of standard DFT exchange−correlation functionals for band gap materials. The intensity ratio difference might have originated from a lack of taking account of the transition dipole moments for photoemission from individual molecular orbitals highly oriented in the assemblies.
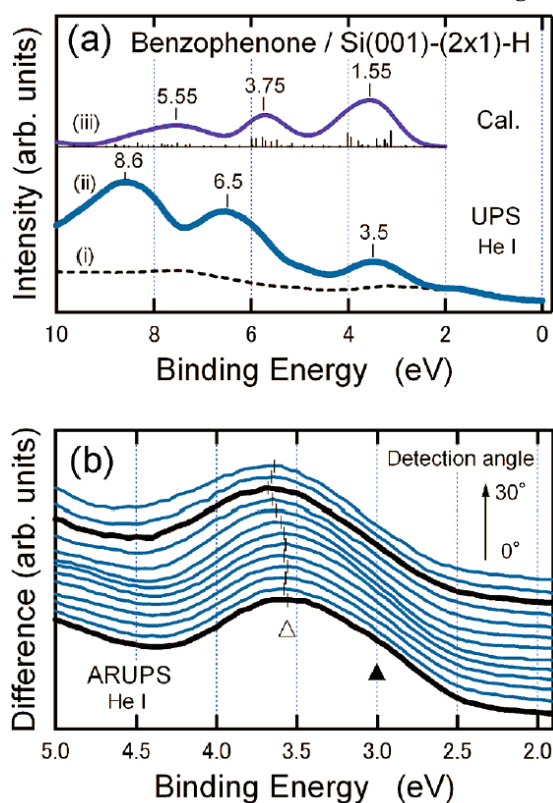
Figure 2. UPS spectra of benzophenone molecular assemblies on Si(001)-(2×1)-H: (a) comparison between measured and calculated spectra; (b) a set of ARUPS spectra. For (a), the spectra of the Si(001)-(2×1)-H surface before (i) and after (ii) the benzophenone dose were detected at the surface normal, and the calculated spectrum (iii) was obtained by the estimated LDOS intensities of the benzophenone assemblies at the Γ point in k-space, with broadening by a Gaussian function of σ = 0.5 eV and an energy shift by +2.0 eV. For (b), the ARUPS spectra were detected at every 2.5° from the surface normal, 0°, to 30° toward the [110] direction. The bold spectra in (b) indicate those at the Γ point and near the first Brillouin zone boundary.

The π–π interaction in the stacking Ph rings was examined by ARUPS measured from the surface normal toward the [110] direction. To ascertain carefully the π–π interaction, particularly the peak at 3.5 eV, the substrate signals were removed by subtraction of the Si(001)-(2×1)-H spectrum from that of the benzophenone-dosed sample following an intensity normalization at the binding energy of 1.2 eV. Figure 2b shows a set of the ARUPS results obtained after the substrate signal subtraction at each detection angle. The shape of peaks in the ARUPS spectra for the benzophenone assembly was

not simply symmetric. At the surface normal detection, the peak was located at about 3.5 eV (open triangle), and a broad shoulder appears at about 3.0 eV (filled triangle). With increasing detection angle, the shoulder decreased in intensity, and the peak was shifted gradually to a deeper binding energy. The spectral change depending on the detection angle reflects an interaction between the stacking Ph π-orbitals in the assembly. The π-orbital interaction in the assembly was evaluated by the calculation of the electronic state dispersion.
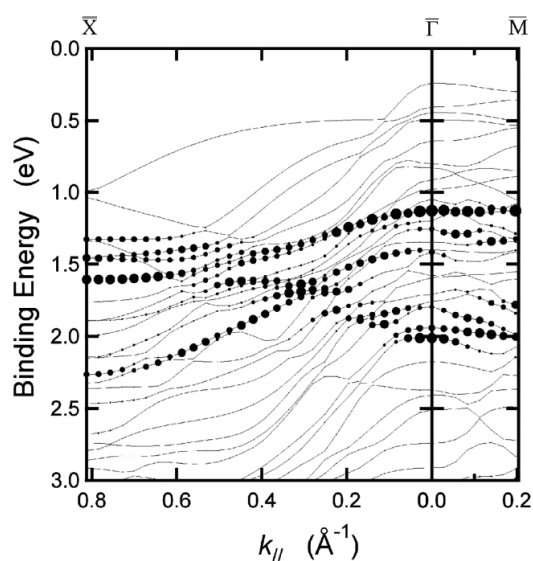

Figure 3. Calculated electronic state dispersion in the k-space for the benzophenone assembly on Si(001)-(2×1)-H using the 4 × 1 supercell shown in Fig. 1c. The thin lines indicate energy levels of the substrate, and the dots describe the energy levels and the LDOS intensity of the benzophenone assembly by their positions and diameters, respectively.

Fig. 3 shows the computed electronic states in the topmost components parallel (toward X) and perpendicular (toward M) to the molecular lines (in the k-space). Several series of dispersive features that originated from the staking Ph orbitals were obtained. In this calculation, the 4 × 1 supercell described in Fig. 1c was used, and thus, the molecular lines are located on every second Si dimer row in the periodic boundary conditions. Though the separation between the molecular lines in this periodicity must be shortest because of the molecular

size, only a small peak shift perpendicular to the lines, that is, little interaction between the molecular lines, was expected. In contrast to that, the energy shift by several sub-eV was estimated parallel to the lines, indicating a strong interaction in the stacking π-orbital range. This dispersion well explains the observed peak features in Fig. 2b. Note that, as shown in Fig. 1d, the HOMO π-state consisting of the stacking Ph rings is isolated from any substrate electronic states, while the next dominant π-state couples to them. Therefore, the dispersion of HOMO at around 1.1 eV in Fig. 3 can be mainly attributed to the π-state delocalization in the stacking Ph rings, without electronic coupling to the substrate.
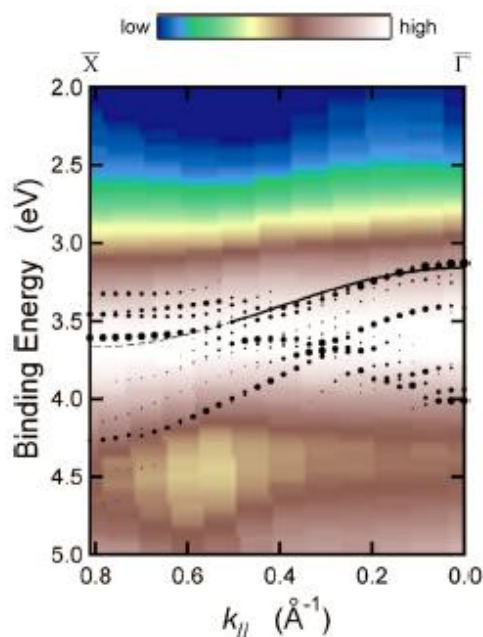

Figure 4. Overlap of the measured and the calculated dispersions for the benzophenone assembly on Si(001)-(2×1)-H. The computed components along the molecular lines were plotted by black circles, with an energy shift of +2.0 eV. Under the TB approximation, the 1D dispersion model is fit to a series of the HOMO states; the fit curve is indicated as the black solid line in the fit area, and the dashed line is for its extension.

Fig. 4 shows the k-space map converted from the ARUPS results in Figure 2b, with the plots of the computed π-state energy levels parallel to the molecular lines in Figure 3 following an energy shift by +2.0 eV. The dispersive band structures along the molecular lines are in good agreement with the observed spectral features; the broad shoulder of about 3.0 eV near the Γ point and the gradual main peak shift to deeper binding energy with increasing $k_\parallel$. Because both molecular lines parallel and perpendicular to the [110] direction, depending on terraces, are included in our ARUPS spectra, the non-dispersive components perpendicular to the molecular lines should overlap and obscure the dispersive features. By the sum of these LDOS components, indeed, the gradual spectral change is well reproduced. To elucidate its properties as a molecular nanowire, fitting of a representative model to the dispersion was performed. Within a simple 1D tight binding (TB) approximation, the energy dispersion is explained as $E_c + 2t \cos(a k_\parallel)$, where E_c, t, and a represent the energy of the band center, transfer integral, and periodicity in the molecular line, respectively. By fitting this equation to a series of the π-orbitals derived from the HOMO, the model reproduces the dispersion as the solid line in Fig. 4 and provides the least-squares fit parameter $t = 0.127$ eV. The effective mass of the holes, m_h, are estimated to be $2.0 m_e$, where m_e is the electron rest mass. This value is comparable to that of the single-crystal molecules providing the high carrier mobility in organic field effect transistors, that is, $1.26 m_e$ at pentacene and $0.65 m_e$ at rubrene. It is, therefore, inferred that the assembled benzophenone lines and possibly the other Ph stacking molecular lines on Si(001)-(2×1)-H have the delocalized electronic states as requisitely demanded for conductive nanowires.

(2) Adsorption-induced stability reversal of photochromic diarylethene on metal surfaces

Considering the potential applications of switching elements and memory devices, immobilization of the photochromic molecules onto solid surfaces is an important step for further advances in organic optoelectronic devices. From the fundamental point

of view, it is also important to understand adsorption configuration and electronic properties of photochromic molecules in contact with solid surfaces at the single molecular level as they provide an insight into the influence of the substrate on quantum efficiency of isomerization reactions, reversibility, fatigue resistance, and thermal stability. Among several types of photochromic molecules, a family of diarylethene (DAE) may have an advantage over azobenzene and spiropyran for application in memory devices because DAE can be designed so that no thermal reaction occurs in solution and single crystalline form. Therefore a lot of efforts have been devoted to the study of DAE molecules attached to solid surfaces mostly focusing on their photochromism using various experimental techniques such as the use of mechanical break-junctions, nanoparticle arrays, and scanning tunneling microscopy (STM). However, a full understanding of adsorption configuration, detailed electronic properties, and relative stability between photochromic isomers has not been achieved yet, in particular for the DAE on noble metals.

In this study, we report on a study of a DAE molecule (hereafter o-DM and c-DM for open- and closed-form isomers, respectively, see Fig. 5f), adsorbed on the Au(111) and Cu(111) surfaces using cryogenic (5 K) ultra-high vacuum STM). The DM studied here is thermally irreversible in its single crystalline form. Single crystalline DM shows a quantum yield for cyclization (close-ring reaction) of almost unity. In solution and the single crystal, the o-DM is more stable than the c-DM.

Deposition of white powder of the o-DM on Au(111) at room temperature (RT) produces two types of protrusions corresponding to single molecules in STM images as shown in Fig. 5a. One has an oval shape and the other appears to be an isosceles triangle, both with a bright spot at the center (see inset of Fig. 5a). After annealing the surface at

355–365 K, almost all the molecules show the triangular shape (Fig. 5b). This observation suggests that the oval-shaped molecules transform into the triangular-shaped molecules by thermal energy. The same phenomenon is also observed on Cu(111) as shown in Fig. 5c–d.
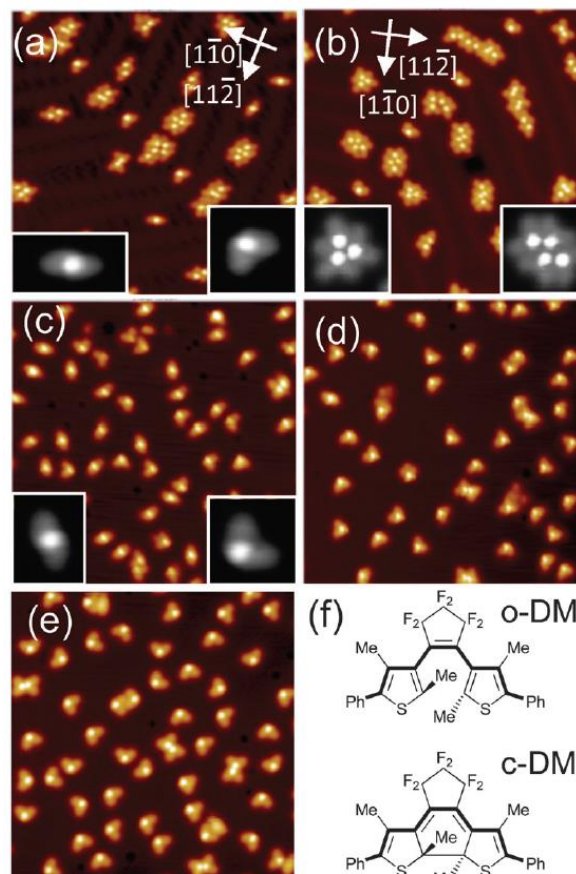

Figure 5. STM images (30 x 30 nm^2) of (a) o-DM deposited on Au(111), (b) followed by annealing to 85 °C. (c) o-DM deposited on Cu(111), (d) followed by annealing to 85 °C. (e) STM image (26 x 26 nm^2) of c-DM deposited at RT. Inset in (a) and (c) are enlarged images of oval shape (o-DM) and triangular shape (c-DM) molecules. Inset in (b) shows enlarged images of trimer and tetramer. (f) Chemical structures of the molecule used in this study, o-DM (upper) and c-DM (bottom). The π-conjugated network along carbon chain connecting two Ph-rings is depicted with bold line. Tunneling parameters are (a, c, d) 1 V, 30 pA; (b) 1 V, 10 pA; (b) inset 1 V, 50 pA; (e) 1 V, 100 pA.

To clarify the relation between molecular conformation and observed STM images, we deposited UV light (375 nm)-exposed powder, which contained mostly dark-blue c-DM, on Cu(111) at RT. We consequently found almost all the molecules to

have a triangular shape (Fig. 5e). This obviously indicates that the triangular-shaped molecules correspond to the c-DM and the oval-shaped ones to the o-DM. It has been known that the thermal isomerization of the DM is prohibited in the gas-phase, solution and the single crystalline form. Thus the extraordinary behavior observed here indicates the reversal in thermodynamic stability of two isomers and significant change in the potential landscape on Au(111) and Cu(111).

In order to support experimental observations on the reversal in thermodynamic stability between the o-DM and c-DM, density functional theory (DFT) calculations were performed for isolated molecules, because more realistic periodic system for single molecule adsorption requires huge size of supercell to separate molecules and thus high computational cost. The PBE0 hybrid density functional was mainly employed to evaluate the relative stabilities between two structural isomers, o-DM and c-DM, for neutral ($Q_{DM} = 0$), anionic (-1) and cationic (+1) states. The optimization of molecular structures and the evaluation of relative energies were carried out using 6-311G(d,p) and 6-311G+(2d,p) basis sets, respectively. The other two hybrid functionals, M06-2X and CAM-B3LYP, were also utilized to check the validity of PBE0 results. All calculations were performed using Gaussian09 program suite. Our computational results indicate that the c-DM becomes more stable than the o-DM by about 7 kcal/mol for both cationic and anionic states although at neutral state, the o-DM is more stable than the c-DM by about 12 kcal/mol (see Table 1). The other functionals, M06-2X and CAM-B3LYP, also consistently yield the reversal of thermodynamic stability between the two isomers by the change in ionic state.
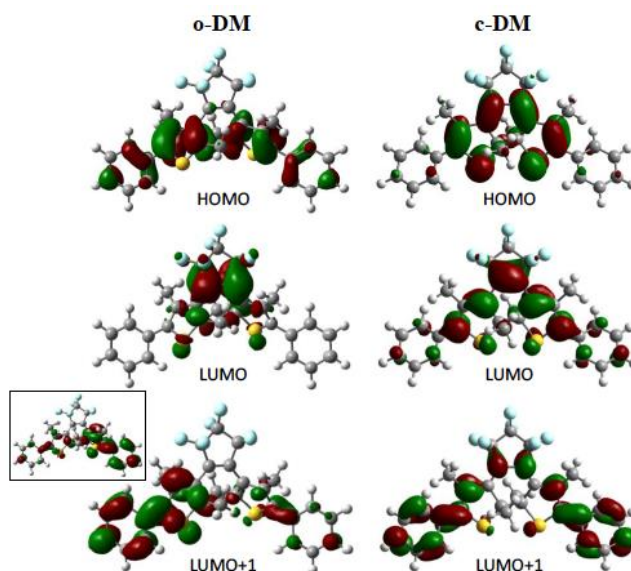

Figure 6. Distribution of HOMO, LUMO, and LUMO+1 for neutral o-DM and c-DM. Doubly-delocalized orbital distribution for the LUMO+1 of o-DM is indicated in inset.
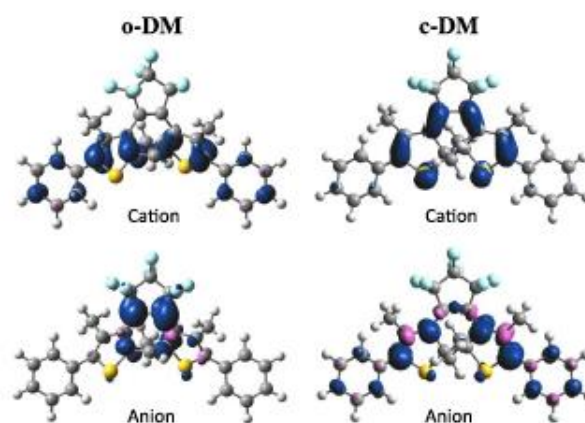

Figure 7. Spin density distribution of o-DM and c-DM at cationic and anionic states.

The isomerization between the o-DM to c-DM induces significant change in π-conjugated network within a molecule as shown in Fig. 6. The distributions of the frontier molecular orbitals, i.e., highest occupied molecular orbital (HOMO) and lowest unoccupied molecular orbital (LUMO), display the different π-conjugated network of two isomers; i.e., both the HOMO of the o-DM and the LUMO of c-DM show wider distribution which extends to the terminal Ph-rings. Therefore, we suppose different change in the π-conjugated nature of each isomer at both cationic and anionic states.

The spin density distributions of both isomers at cationic and anionic states show close correlation with the HOMO and LUMO, respectively (see Fig. 7).

	Neutral		Anion		Cation	
	o-DM	c-DM	o-DM	c-DM	o-DM	c-DM
Relative energy (kcal mol^{-1})	0.00	11.83	7.35	0.00	7.23	0.00
$\sigma(d_{C-C})$ (Å)	0.048	0.048	0.040	0.026	0.036	0.026
σ(WBI)	0.267	0.234	0.184	0.120	0.216	0.100

Table 1. Calculated relative energies (kcal/mol) between two isomers (o-DM and c-DM), and standard deviations for C–C bond length, $\sigma(d_{C-C})$, and corresponding Wiberg bond index (WBI), σ(WBI), along the carbon chain connecting two terminal Ph-rings at neutral, anionic and cationic states.

To investigate the order of change in π-conjugated network within a molecule, we examine C-C bond lengths (d_{C-C}) and corresponding Wiberg bond indices (WBI) along carbon chains connecting two terminal Ph-rings (see Fig. 5f) because highly conjugated system should lead to a small deviation in bond lengths and WBI. Table 1 show the standard deviations (σ) for the d_{C-C} and WBI. At both cationic and anionic states, the larger decreases in $\sigma(d_{C-C})$ and σ(WBI) for the c-DM than the o-DM clearly indicate the formation of more effective π-conjugated network in the c-DM compared to the o-DM. Therefore, we suggest that this noticeable change in the stability depending on the ionic state can be interpreted using the different influence on the π-conjugated network.

In addition, we performed the calculations to evaluate the changes in barrier height for the isomerization from o-DM to c-DM depending on the ionic state. The geometry of transition state (TS) for neutral molecule at ground state (S_0) was also optimized using spin unrestricted DFT calculations because the transition state at neutral state may have a diradical character. Therefore, in order to get rid of the error due to spin contamination, we employed the approximate spin-correction procedure proposed by Yamaguchi et al. [Chem. Phys. Lett., 148, 537 (1998)], in which the contamination of the singlet wavefunction is assumed to be contributed only from the first triplet state (T_1). Our calculations also reveal that the reaction barriers for the cyclization are significantly reduced by 1.0 and 1.1 eV for the anionic and cationic states, respectively, compared to that of neutral state (2.0 eV). This also supports the thermal isomerization demonstrated in Fig. 5.

(3) Molecular Assembly Through the Chain Reaction of Substituted Acenes on the Si(100)−(2×1)−H Surface

Regarding 1D molecular assemblies on the H-terminated Si(001)-(2×1) surface, we have investigated the formation of molecular assemblies by some commercially available small molecules of the acene family (as shown in Fig. 8) through the dangling bond initiated chain reaction in ultrahigh vacuum (UHV) at room temperature.
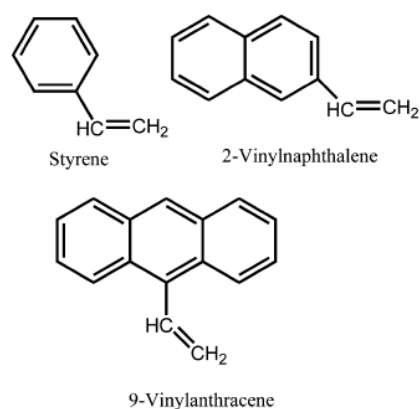

Figure 8. Molecules investigated in the present study.

The assemblies formed by acene molecules on the surface are investigated by an in situ scanning tunneling microscope. The 2-vinylnaphthalene molecules undergo a chain reaction similar to that of styrene leading to the 1D molecular assembly along the dimer-row on the surface (Fig. 9a and 9b). Unlike styrene and 2-vinylnaphthalene, the

9-vinylanthracene molecules form both ordered and disordered assemblies on the surface (Fig. 9c). The ordered assembly is similar to that of styrene assembly running along the dimer-row (Fig. 9d). One can see that the 1D structure seen in Fig. 9d no longer exists in the next image shown as Fig. 9e. After the disappearance of the 1D structure, the underlying H-terminated dimer-row is clearly seen in Fig. 9e. This suggests that a reversed chain reaction leading to the desorption of all chemisorbed molecules in the 1D assembly happens even at room temperature. This spontaneous reversed chain reaction at RT suggests that a significant repulsive interaction due to steric hindrance exists among the aligned molecules, which makes such ordered assembly by 9-vinylanthracene less stable.
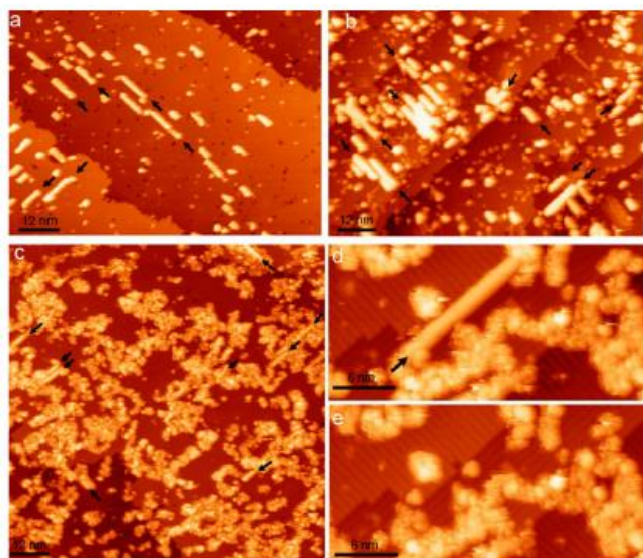

Figure 9. STM images of molecular assemblies formed on the H-terminated Si(100)-(2×1) surface by exposure to (a) ~20 L of styrene, (b) ~100 L of 2-vinylnaphthalene, and (c) ~100 L of 9-vinylanthracene molecules at RT. Typical one-dimensional (1D) assemblies formed by these molecules along the dimer-row are indicated. The (d) and (e) are the same area STM images acquired sequentially demonstrating the disappearance of a 1D molecular assembly formed by 9-vinylanthracene through the reversed chain reaction. (a,c) V_s = -2.2 V; (b) V_s = -3.0 V; (d,e) V_s = -2.5 V; I_t = 0.2 nA.
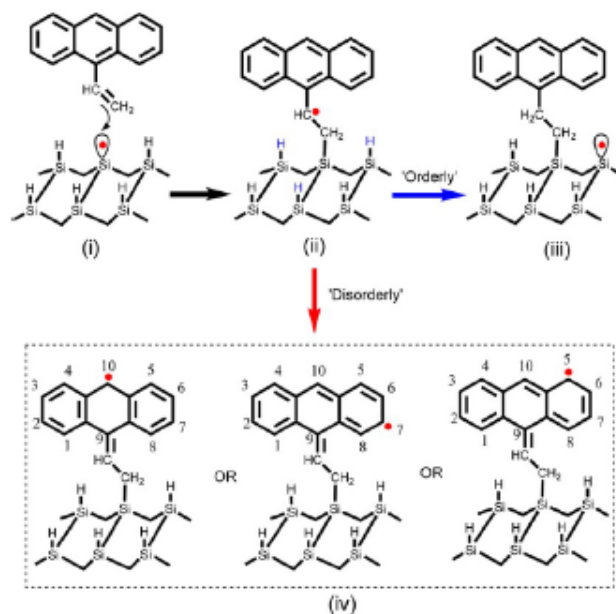

Figure 10. (i–iv) Possible chain reaction mechanism for 9-vinylanthracene molecules with the dangling bond site of the Si(100)-(2×1)-H surface leading to the ordered and disordered patterns. (i) Initial reaction of the 9-vinylanthracene molecule with the dangling bond (BD) site of the surface. (ii) The C-centered intermediate radical generated after initial reaction. (iii) A new DB site is created through abstraction of the nearby surface H by the C-centered intermediate radical. (iv) Three of several possible C radicals that can form through the resonance structure of anthracene.

The differences in forming either ordered or disordered assembly depend on the characteristics of intermediate C radical [as in Fig. 10(ii)]. In a normal chain reaction mechanism, if the intermediate C radical abstracts the surface H atom from the same dimer-row resulting in a new radical site [as in Fig. 10(iii)], the reaction proceed along the dimer-row direction forming a 1D assembly as observed in the case of styrene, 2-vinylnaphthalene, and ordered assembly of 9-vinylanthracene molecules (Fig. 9). Note that the C radical in (ii) can only reach to the nearest H of the same row (blue colored H). Indeed the formation of a disordered assembly cannot be accounted for by the reaction proceeding through the abstraction of H by the C radical shown in Fig. 10(ii). It has been reported that abstraction of the surface H leading to the formation of the nanostructure depends on the stabilization of the C-centered

intermediate radical. Hence we suggest that the initial intermediate C radical is transferred on the phenyl C atom through the resonance structure in the case of 9-vinylanthracene; that is, a C radical may be localized at '7, 5, 10, or other' positions of anthracene skeletal [Fig. 10(iv)].

Unrestricted density functional theory (DFT) calculations were performed to see the spin density distribution of intermediate radical states formed by styrene, 2-vinylnalphthalene, and 9-vinylanthracene adsorbed on a simple H-terminated Si_9 cluster. We employed the PBE0 hybrid density functional implemented in the Guassian09 program suite. The optimization of molecular structures and the detailed evaluation of electronic structures were carried out using 6-31G(d,p) and 6-311G(2d,p) basis sets, respectively. The DFT calculation results as shown in Fig. 11 suggest that, although the relative spin density is dominant at the vinyl C atom for styrene and 2-vinylnaphthalene, it is at the phenyl C(10) position in the case of 9-vinylanthracene molecules. Now it can be realized that the C(10) radical can reach the surface H even from the nearby dimer-row and, hence, can abstract any of the several surface H atoms around the anchored Si−C bond leading to the formation of disordered assembly.
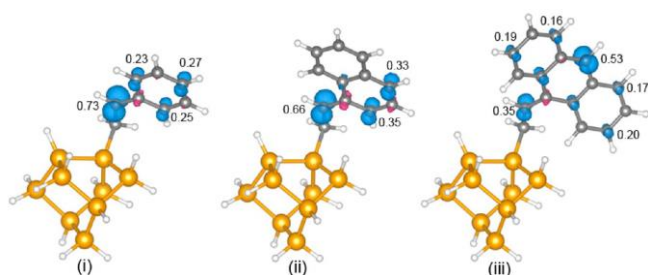

Figure 11. Spin density distribution obtained by DFT calculation for intermediate radicals formed by the interaction of (i) styrene, (ii) 2-vinylnaphthalene, and (iii) 9-vinylanthracene molecules with a dangling bond of the H-terminated Si_9 cluster. The numerical values of Mulliken atomic spin densities (e) for selected C atoms are indicated.

(4) Mode-selective electron-phonon coupling in laser photoemission on Cu(110)

With improvements in energy resolution of photoemission spectroscopy, which is one of the most reliable tools for determining electronic band structures, several signals originating from the electron-phonon interactions have appeared in the spectrum apart from the vibrational progression structure in gas-phase experiments. Two well-known examples are the 'kink' structure around the Fermi wavenumber in the electronic band dispersion of metallic and superconducting systems determined with angle resolved photoemission experiments [M. Hengsberger et al., Phys. Rev. Lett. 83, 592 (1999)] and the linewidth broadening of the noble metal surface states as a function of temperature [P. Hofmann et al., Phys. Rev. B 66, 245422 (2002)]. Both of them have been described by the electron self-energy attributable to the electron-phonon coupling around the Fermi level (E_F).
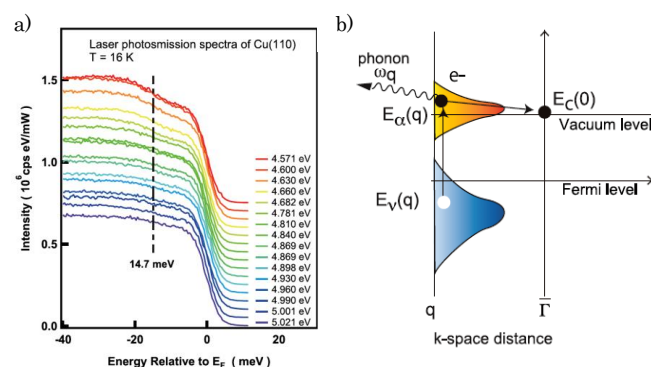

Figure 12. (a) LPES of the clean Cu(110) surface excited by the laser photon from 4.571 to 5.021 eV. The sample temperature is 16 K. (b) Schematic diagram of the indirect excitation in LPES.

Recently, a completely different manifestation of electron-phonon coupling, inelastically scattered photoelectron by phonons, was observed in low-energy photoemission spectra. Fig. 12a shows laser photoemission spectroscopy (LPES) results of Cu(110) [R. Arafune et al., Phys. Rev. B 80, 073407 (2009)], which we investigated in detail. In

addition to the Fermi-Dirac distribution curve originating from the elastic process, a single step structure appeared at 14.7 meV below E_F, which implies that the detected photoelectrons lose their energy through coupling with particular phonon modes. In our experiment, the photoelectrons were emitted from the Γ point in the surface Brillouin zone (SBZ), because photoemission spectra were measured in the normal-emission geometry. Therefore, the inelastic photoemission process is expected to be an indirect excitation process in which electrons of wavevector q couple with phonons of the same wavevector and scatter to the Γ point, as shown schematically in Fig. 12b. We investigate this indirect excitation process using ab-initio calculations which includes electron-phonon coupling calculations based on the density functional perturbation theory (DFPT).
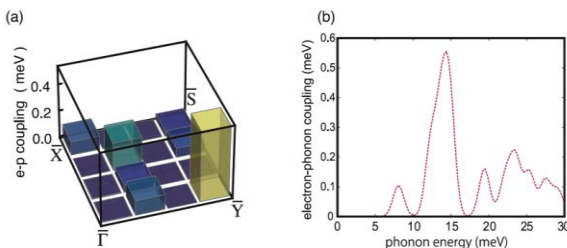

Figure 13. (a) Calculated electron-phonon coupling matrix element with a phonon energy of 14.7 meV, which induces photoelectron scattering from the k-point with wavevector q to the Γ point. (b) Electron-phonon coupling spectrum at the Y point as a function of the phonon energy.

The electron-phonon coupling is the governing parameter in the inelastic scattering process. Fig. 13a shows the electron-phonon coupling at the vacuum level (E_V) with 14.7 meV phonon energy on 16 irreducible points of a 6x6x1 grid in SBZ. One would see that the electron-phonon coupling has minor value at every k-point except for the Y point. The electron-phonon coupling spectrum as a function of the phonon energy should have a main peak around 14.7 meV because the step appears at this

energy in the LPES result. As shown in Fig. 13b, the spectrum at the Y point contains a peak around 14.7 meV. Thus, we have judged that the inelastic signal in the LPES result of Cu(110) originates from the indirect excitation process from the Y to the Γ point.

An inspection of the phonon modes around 15 meV at the Y point shows that the phonon modes polarized along the $[\bar{1}10]$ direction exhibit high density of states in the second and deeper layers, in spite of the low density of states in the topmost layer. Among them, we observe that four modes polarized along the $[\bar{1}10]$ direction with phonon energies of 13.45, 13.67, 14.63, and 14.83 meV have large electron-phonon matrix elements and are the source of the main peak at the Y point in Fig. 13b. We found that these four modes are subsurface phonons [E. Minamitani et al., Phys. Rev. B, 88, 224301 (2013)].

Subsurface phonons have recently been detected through Helium atom scattering (HAS) experiments. We note here that the mechanism of the subsurface phonon excitation in HAS differs from that in LPES experiments, which is elucidated in the following. Subsurface phonon excitation in HAS is due to the strong charge oscillation at surfaces caused by the subsurface phonon mode [V. Chis et al., Phys. Rev. Lett. 101, 206102 (2008)], which is totally different from the LPES experiments. In fact, the shear horizontal phonon modes that correspond to that polarized along the $[\bar{1}10]$ direction in this study do not contribute significantly in HAS, although they appeared in the LPES results. High resolution electron energy loss spectroscopy (HREELS) experiments could be used to probe the subsurface phonon, because the electron in the inelastic impact regime may be scattered by the atom core oscillation in the first few layers. However, the 14.7 meV loss has not been observed in the HREELS spectra. It would be extremely interesting to extract the essences of the theory that predicts the inelastic photoemission by taking the difference between

HREELS and LPES into consideration. Although the exact origin of the difference between HREELS and LPES is not completely clear, we have succeeded in demonstrating that the laser photoelectron excites the subsurface phonon; the current results also indicate that the LPES experiments provide a novel means for the characterization of subsurface phonons.

(5) Direct observation of adsorption geometry for the van der Waals adsorption of a single π-conjugated hydrocarbon molecule on Au(111)

Weak van der Waals (vdW) adsorption of π-conjugated hydrocarbon (π-CHC) molecules onto the gold surface, Au(111), is one of the essential processes in constructing organic-metal interfaces in organic electronics. Here we provide a first direct observation of adsorption geometry of a single π-CHC molecule on Au(111) using an atomically resolved STM study combined with vdW density functional methodology. For the purpose, we utilized a highly symmetric π-CHC molecule, dehydrobenzo[12]annulene (DBA), which has a definite three-fold symmetry, the same as the Au(111) surface.

Figures 14a-c show high-resolution STM images of the isolated single DBA molecule on the Au(111) surface, which clearly demonstrates that the center of the DBA molecule resides in a hollow site in a planar fashion similar to other π-CHC molecules. Low-coverage deposition at RT prevents lateral interaction between adsorbates and enables the reliable detection of the proper geometry of DBA at the single-molecule level. Two different types of surface scanning at atomic resolution, i.e., spatially varying the tunneling conditions in the vicinity of the adsorbate (Fig. 14a) and dragging the adsorbate with the STM tip (Fig. 14b and 14c), were performed to accurately observe the adsorption geometry of

DBA/Au(111). Fig. 14d shows mirror-symmetry axes in the molecular plane displaced from the <112> surface axes, which results in reduced symmetry of the DBA/Au(111) system from C_{3v} to C_3. Because all DBA molecules have identical adsorption geometry and exhibit two molecular orientations in enantiomorphous forms with respect to the Au(111) surface, as shown in Fig. 14e, the two molecular orientations created by the single adsorption event on the surface display single-molecule chirality, i.e., single-molecule alignment breaks the reflection symmetry axes of the surface.
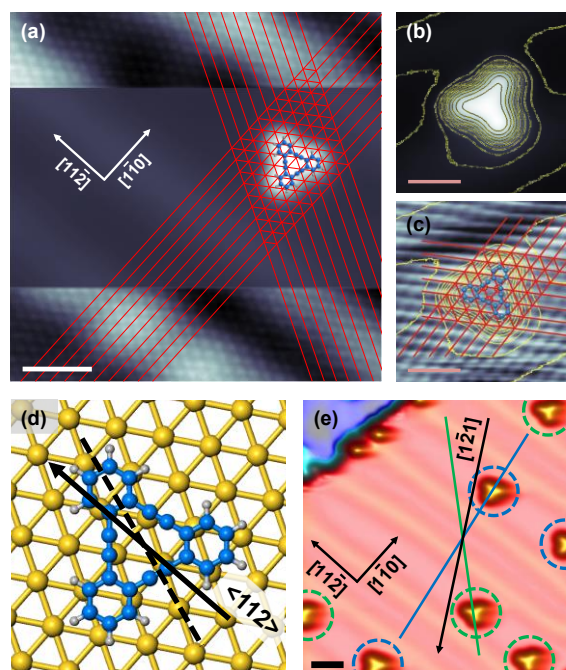

Figure 14. (a) STM image of isolated DBA molecule on Au(111) obtained by spatially varying the tunneling conditions. (b) STM image of DBA/Au(111) before dragging the molecule. (c) STM image obtained at the same location as (b) via dragging the molecule. Contour lines of (b) are superimposed on (c), which precisely presents the locations of the Au atoms beneath the DBA molecule of (b). (d) Optimized structure of DBA/Au(111) by vdW-DF calculation (C, blue; H, grey; Au, yellow). (e) Low-coverage STM image for the DBA adsorption on Au(111). Green and blue dashed circles indicate two molecular orientations of DBA in enantiomorphous forms with respect to the <112> surface axes

Our STM experiments provide a good opportunity to

unveil the correlation between adsorption geometry and interfacial electronic structures in weak adsorption of a π-CHC molecule on Au(111) with the aid of computational methods. Thus, we performed periodic vdW-DF calculations for the adsorption of DBA, of which the center resides in a hollow site of Au(111), based on the experimental results. The periodic vdW-DF calculations were performed with the optB86b-vdW functional implemented in the Vienna Ab-initio Simulation Package (VASP) code, which not only yielded a more accurate lattice constant of various solids than the originally proposed revPBE-vdW functional but was also successfully applied to describe the interfacial interaction between graphene and metal substrates. Core electrons were replaced by projector-augmented wave (PAW) pseudopotential, expanded in a basis set of plane waves up to the cut-off energy of 400 eV. In order to focus on the isolated single DBA molecule without lateral interaction among neighboring adsorbates on the surface, large (6×6) supercells and 4×4×1 Γ-centered k-point grid were used for its Brillouin zone sampling. The slab model consists of six Au layers (216 atoms) with the two bottom Au layers fixed in their bulk positions during ionic relaxations. The periodically replicated slabs were separated by a vacuum region of ~19 Å. The convergence criteria for the electronic self-consistent iterations and ionic relaxations were 10^{-7} eV and 0.01 eV/Å, respectively. In addition, Bader population analysis was performed to calculate the resultant charge transfer between the DBA molecule and Au(111) surface. We note here that the optimized structure of DBA/Au(111) provides excellent agreement with the STM images (see Fig. 1d), where the optimized displacement angle of DBA with respect to the <112> surface axes is 20°.

The DBA/Au(111) system was examined to have weak vdW adsorption characteristics by means of STS and vdW-DF calculations. Since this weak adsorption does not quench the surface state, the

Au(111) Shockley surface state near the Fermi level (E_F) is still clearly shown over the adsorbate and is also slightly shifted toward the E_F in the STS spectra as shown in Fig. 15.
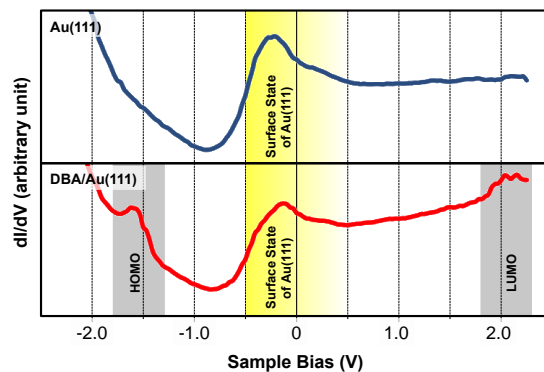

Figure 15. STS spectra of (top) the bare Au(111) surface and (bottom) the DBA molecule on Au(111).

Our vdW-DF calculations do not indicate a significant structural change nor distortion of DBA upon adsorption to the Au(111) surface, where the changes in bond length and planarity accompanied by the adsorption process are less than 0.01 and 0.1 Å, respectively. Adsorption energy (E_a) of DBA/Au(111) calculated using the optB86b-vdW functional is 2.74 eV, which was highly comparable to the recent computational result for benzene/Au(111), one of the prototype weak vdW adsorption systems. The authors reported the adsorption energy of benzene/Au(111) is 0.86 eV using the same vdW-DF methodology (optB86b-vdW). Considering a ratio of the vdW surface area of DBA with respect to that of benzene is 2.97, the E_a for DBA/Au(111) of 2.74 eV [E_a(DBA)/E_a(benzene) = 3.19] supports that DBA/Au(111) is regarded as a weak vdW adsorption system, which is also comparable to those of other well-known weak adsorption systems, such as 2.51 eV and 1.66 eV for pentacene/Au(111) calculated by DFT-D and vdW-DF (using the revPBE-vdW functional) methodologies, respectively. The reported adsorption distance of benzene/Au(111) (~3.04 Å) is also comparable to that of DBA/Au(111) (~3.11 Å). In addition, DBA/Au(111) was recalculated using

semilocal PBE functional, which resulted in the E_a of 0.18 eV and the adsorption distance of 3.75 Å. These results indicate that the vdW interaction mainly contributes to the adsorption process of DBA on the Au(111) surface. Our experimental and computational results obviously show that DBA/Au(111) is a weak adsorption system via vdW interaction.
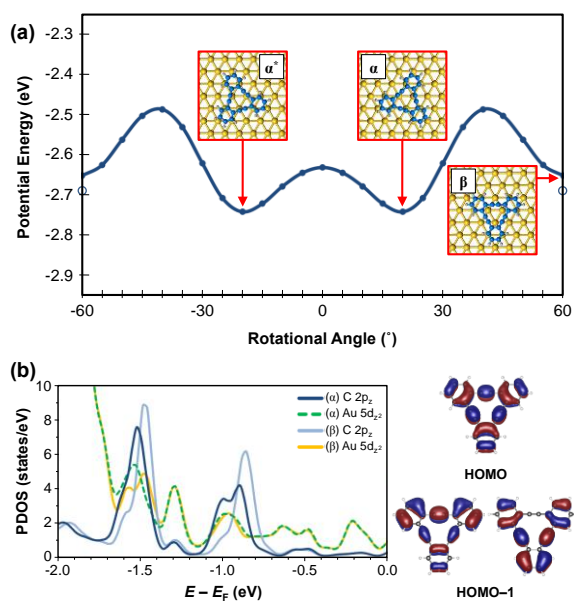

Figure 16. (a) Potential energies due to the horizontal rotation of DBA on Au(111) with respect to the <112> surface axes. Open circles at ±60° indicate the potential energy of optimized β geometry. Potential energies are computed relative to E(DBA) + E(Substrate) = 0 eV. α* indicates the chiral structure of α. (b) PDOS diagrams for the occupied π-states (C 2p$_z$), the HOMO and the doubly degenerated HOMO–1 states, of both α and β local minima with the z-component of 5d state of Au(111). The z-component of Au 5d and C 2p$_z$ states were plotted for the two Au layers from the surface and the carbon atoms of DBA, respectively. The spatial distributions of π orbitals are also depicted at the right side of (b). The molecular orbitals of the DBA molecule were calculated using the PBE/cc-pVTZ method to characterize the electronic structure of DBA near the E_F, which presented the almost identical electron density distribution to the partial charge density distribution obtained from periodic vdW-DF calculations

To gain deeper insight into the interplay between DBA and the Au(111) surface within the vdW framework, the E_a variance in response to horizontal rotation of the DBA molecule was calculated. Fig. 16a shows the calculated adsorption energies corresponding to various molecular orientations rotated by 5° increments with respect to a rotational symmetry axis of the DBA molecule on Au(111), indicating two non-equivalent local minima. The experimentally observed adsorption structure (designated "α" and "α*"; α* is the chiral structure of α) with C_3 symmetry is most favorable with the highest E_a of 2.74 eV, which is followed by a second local minimum (designated "β", obtained by optimization) with C_{3v} symmetry and an E_a of 2.70 eV. The adsorption distance of β geometry (3.20 Å) is slightly longer than that of α geometry by 0.09 Å. Each projected DOS (PDOS) of the two local minima (α and β) was investigated to clarify a correlation between the adsorption geometry and the interfacial electronic structure of DBA/Au(111) as shown in Fig. 16b. The first (~–0.9 eV) and second (~–1.5 eV) peaks originating from the DBA molecule in the PDOS diagrams correspond to the HOMO and the doubly degenerated HOMO–1 states of DBA, respectively. The spatial distributions of π orbitals for both HOMO and HOMO–1 states represent a highly conjugated character of the DBA molecule. We found that the difference in adsorption strengths of the two local minima can originate from the degree of overlap between the π-state of DBA and the z-component of 5d state of the Au(111) surface, which leads to the π-state broadening according to the Newns-Anderson scheme. As indicated in Fig. 16b, both HOMO and HOMO–1 states of DBA in α geometry are more overlapped with the z component of 5d state of Au(111), compared to β geometry, which strongly suggests that such weak electronic coupling between a π-CHC molecule and the Au(111) surface contributes to constraining the adsorption structure, even for the weak vdW adsorption. Bader population analysis also revealed that a higher orbital overlap results in a relatively larger amount of electron-transfer from DBA to Au(111): the resultant electron-transfer for α geometry (0.26e) is

slightly larger than β geometry (0.23e) and the molecular charge varies by ~0.1e during the horizontal rotation, which is in agreement with the relative stability. Note that the STS spectrum of DBA/Au(111) (see Fig. 15) reflects such a static charge transfer from the molecule to the substrate, where the relative position of the HOMO of DBA is closer to the E_F than the LUMO.

4．Conclusion

We have tried to examine a variety of molecular behaviors on the surface. First, the electronic states of the 1D benzophenone molecular assemblies on Si(001)-(2×1)-H were studied using STM, ARUPS, and DFT calculations. The high-resolution STM images corroborated a calculated stable structure in the molecular lines. The dispersive features of its HOMOs were obtained in both ARUPS and calculation results. The dispersive HOMO state was expected to be the hole effective mass of 2.0me, which ensured the delocalized electronic states requisitely demanded for a molecular charge transport wire. Second, we have clarified adsorption behavior of one of DAE molecules on Au(111) and Cu(111) using STM and DFT at the single molecular level. Thermal cyclization reaction was clearly observed and we propose the following scenario as its reason: the o-DM is partially ionized when adsorbed on Au(111) or Cu(111) because of the charge transfer and/or hybridization. It lowers the reaction barrier for the cyclization reaction, which is now enough to be overcome by thermal energy. Third, DFT calculation results revealed that the formation of and disordered assemblies by 9-vinylanthracene molecules is ascribed to the resonance structure of the C centered intermediate radical generated by the reaction of the molecule with a DB site of the surface. Fourth, DFT+DFPT calculation results first elucidate the origin of characteristic step structure appears in LPES on Cu(110). Because of the

wavenumber dependence of the electron-phonon coupling at vacuum level, only particular phonon modes contributes to the LPES. This mechanism will open up a new way for selective observation of vibration at surface. Finally, our observations of the weak vdW adsorption system clearly indicate that a π-CHC molecule can have a specific adsorption configuration, even on the noble Au surface. Based on the precisely determined adsorption geometry of DBA/Au(111), the vdW-DF calculations provide improved knowledge of orbital interactions at the interface between a π-CHC molecule and the Au(111) surface. Such interfacial orbital interaction originates from the weak electronic coupling between the molecular π-state and the electronic states of the Au surface, which can play a decisive role in constraining adsorption geometry even in the archetypal vdW adsorption system. Our study provides new perspectives to organic electronics using π-CHC molecules on the Au surface.

5．Schedule and prospect for the future

(1) Controlling chemical reactivity of ultrathin oxide film

Ultrathin oxide film grown on metal substrate has been a subject of great interest not only as a supporting material for chemically active nanoparticles but also as a catalyst in the field of heterogeneous catalysis, where it provides various ways to control the properties of adsorbates via following factors (See Fig. 17): (i) charge transfer between adsorbates and oxide-metal interface, which is closely correlated with the electronic affinity (EA) of adsorbate and workfunction reduction, (ii) adhesion between oxide and metal layers with strong polaronic distortion, (iii) film thickness, and (iv) the chemical composition of oxide surface.
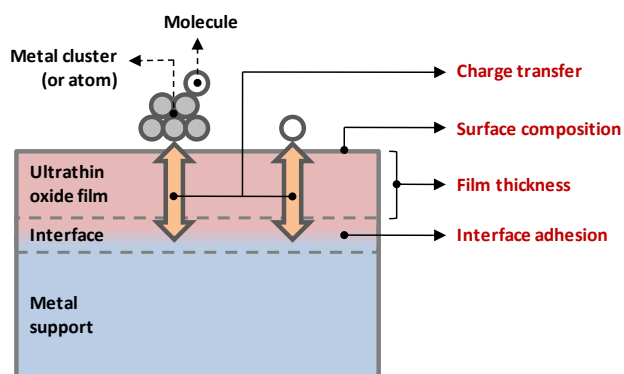
Figure 17. Schematic diagram for heterogeneous catalyst using ultrathin oxide film.

Therefore, we will continue our work to find the way for controlling the chemical reactivity using theoretical and experimental studies. In FY2014, we will extend our study into O_2 dissociation on MgO/Ag(100) with the interface dopants using combined STM and DFT methodology. In the case of O_2 dissociation on MgO/Ag(100), we should consider an influence from the charge redistribution between the oxide-metal interface and the adsorbate, because of O_2 has much higher EA than that of H_2O molecule. The other branch of our study is the clear understanding of the drawing effect at the oxide-metal interface, which can enhance the concentration of dopants at the interface. We believe that our study provides not only profound insight into the chemical reactivity control of ultrathin oxide film but also an impetus for investigating ultrathin oxide films for a wider range of applications.

(2) Molecular adsorption on solid surface: From single molecule to molecular network

We have recently examined a variety of molecular architectures on Au(111) using combined STM and DFT calculations. For study on the adsorption of single molecules on metal substrate, we suggested the origin of adsorption-induced stability reversal of photochromic DAE on metal surfaces and revealed that the interfacial orbital interaction originated from the weak electronic coupling between the molecular π-state and the electronic states of the Au surface can play a decisive role in constraining adsorption geometry even in the archetypal vdW adsorption system. For the molecular architectures formed on the surface, we studied an azobenzene derivative with two designed functional groups of different chain lengths to demonstrate a 1D molecular zipper. The formation and underlying mechanism of the molecular zipper resulted from combined hydrogen bonding and vdW interaction between adjacent molecules, investigated on the Au(111) surface. As the other 1D systems, the formation and electronic structure of 1D molecular assemblies formed on Si(001)-(2×1)-H were extensively studied by DFT calculations. In particular, dispersive feature along 1D benzophenone assembly is deeply examined by periodic DFT calculations. The influence of the balance between hydrogen bonding and vdW interactions on the formation of 2-D molecular network on the Au(111) was also investigated using alkoxylated derivatives of triangular dehydrobenzo[12]annulene (DBA) as building blocks. The relative importance of intermolecular hydrogen bonding versus vdW interactions depends on the length of the alkoxy groups. Such tunable intermolecular interactions balanced with surface–molecule interaction may eventually enable control of the formation of 2D molecular networks. In addition, a 2-D fluorinated fullerene ($C_{60}F_{36}$) superstructure was successfully fabricated on Au(111) in a well-ordered manner and investigated to reveal the driving force toward commensurate molecular film formation. The difference in the lowest unoccupied molecular orbital (LUMO) distribution among three isomers (C_3, C_1, and T) of $C_{60}F_{36}$ suggests that a well-ordered monolayer consists of only C_3 isomer, and the adsorption orientation is determined by localized distribution of its LUMO. Intermolecular C–F…π electrostatic interactions are other important factors in the

formation of the superstructure.

Our results suggest that knowledge of molecule-molecule and molecule-substrate interactions and their balance, even on the noblest gold substrate, is of great importance to understand the formation mechanisms of various molecular architectures and further, to help determine the direction for efforts to design and control them for use in the future development of nano-structured molecular devices. In particular, we will continue the research for a variety of molecular assemblies on the surfaces as follows: (1) various π-conjugated molecules on solid surfaces, (2) 1-D superstructure formation of DAE molecule with NaCl co-deposition, and (3) phthalocyanine on insulating filme surface grown metal substrate).

(3) Electronic structures of functionalized graphene grown on metal substrate

Functionalization of graphene has received great attention not only in fundamental research but also in tuning the physical and chemical properties of graphene sheet, such as opening band gap to achieve semiconducting nature and increasing chemical adaptability for integrating graphene as a building block into a variety of functional materials. Atomic functionalization on the basal plane of graphene with covalent bond is one of the main braches to achieve novel property of graphene, in which hydrogen, fluorine and oxygen have been extensively studied as a key species in order to induce symmetry breaking of graphene composed of sp^2 hybridized carbons. In FY2014, we are going to study the way to achieve the homogeneous functionalization of graphene with combined experiment-theory approach.

(4) Electron-phonon coupling at surface

In this fiscal year, we have developed the theoretical method to investigate the electron-phonon coupling at surface. As results, we elucidated that the characteristic step structure in laser-photoemission spectra (LPES) on Cu(110) originated from electron-phonon coupling between subsurface phonon and photoelectron. Our results indicate the possibilities of LPES as a novel vibrational spectroscopy for the phonons hidden beneath the surface. In FY2014, we are going to extend this study to the molecular adsorbed system and layered material such as graphene.

Fiscal Year 2013List of Publications Resulting from the Use of RICC

* The members registered as the user of RICC system in FY2013 are indicated by underline.

[Publication]

1. S. Kamakura, <u>J. Jung</u>, T. Minato, <u>Y. Kim</u>, M. Z. Hossain, H. S. Kato, T. Munakata, and M. Kawai, "Dispersive electronic states of the π-orbitals stacking in single molecular lines on the Si(001)-(2×1)-H surface", *J. Phys. Chem. Lett.*, **4**, 1199 (Apr. 2013).

2. T. K. Shimizu, <u>J. Jung</u>, <u>H. Imada</u>, and <u>Y. Kim</u>, "Adsorption-induced stability reversal of photochromic diarylethene on metal surfaces", *Chem. Commun.*, 4**9**, 8710 (Aug. 2013).

3. M. Z. Hossain, H. S. Kato, <u>J. Jung</u>, <u>Y. Kim</u>, and M. Kawai, "Molecular assembly through the chain reaction of substituted acenes on the Si(100)-(2×1)-H surface", *J. Phys. Chem. C*, **117**, 19436 (Sep. 2013).

4. <u>E. Minamitani</u>, R. Arafune, M. Q. Yamamoto, N. Takagi, M. Kawai, and <u>Y. Kim</u>, "Mode-selective electron-phonon coupling in laser photoemission on Cu(110)", *Phys. Rev. B*, 88, 224301 (Dec. 2013).

5. J.-H. Kim, <u>J. Jung</u>, K. Tahara, Y. Tobe, <u>Y. Kim</u>, and M. Kawai, "Direct observation of adsorption geometry for the van der Waals adsorption of a single π-conjugated hydrocarbon molecule on Au(111)", *J. Chem. Phys.*, **140**, 074709 (Feb. 2014).

[Oral presentation at an international symposium]

1. <u>Y. Kim</u>, "Interface tuning of an ultrathin MgO film for controlling chemical reactivity", The 24th International Conference on Molecular Electronics & Devices (IC-ME&D 2013), Daejeon, Korea (May. 2013). (Invited)

2. <u>Y. Kim</u>, <u>J. Jung</u>, H.-J. Shin, and M. Kawai, "Single molecule chemistry on an ultrathin MgO film", 19th International Vacuum Congress (IVC-19), Paris, France (Sep. 2013).

3. <u>E. Minamitani</u>, R. Arafune, N. Takagi, M. Kawai, and <u>Y. Kim</u>, "The photoelectron and phonon interaction at the Cu(110) surface", 19th International Vacuum Congress (IVC-19), Paris, France (Sep. 2013).

4. <u>Y. Kim</u>, "Single molecule chemistry with an STM", NSYSU-RIKEN Joint Workshop, RIKEN, Japan (Oct. 2013). (Invited)

5. <u>Y. Kim</u>, <u>J. Jung</u>, H.-J. Shin, and M. Kawai "Controlling surface reactivity of an ultrathin MgO film by interface tuning", American Vacuum Society (AVS) 60th International Symposium and Exhibition, Long Beach, California, USA (Oct.-Nov. 2013).

6. <u>M. Imai</u>, <u>H. Imada</u>, T. K. Shimizu, M. Kawai, and <u>Y. Kim</u>, "Electronic structure of H2Pc on ultrathin NaCl films with various thickness", American Vacuum Society (AVS) 60th International Symposium and Exhibition, Long Beach, California, USA (Oct.-Nov. 2013).

7. T. K. Shimizu, <u>J. Jung</u>, <u>H. Imada</u>, and <u>Y. Kim</u>, "Stability reversal and superstructure formation of photochromic diarylethene on noble metals", American Vacuum Society (AVS) 60th International Symposium and Exhibition, Long Beach, California, USA (Oct.-Nov. 2013).

8. J. Jung, H.-J. Kim, K. Tahara, Y. Tobe, M. Kawai, and Y. Kim, "Formation mechanism of van der Waals interface between a π-conjugated molecule and Au(111)", American Vacuum Society (AVS) 60th International Symposium and Exhibition, Long Beach, California, USA (Oct.-Nov. 2013).

9. H. Imada, M. Imai, T. K. Shimizu, M. Kawai, and Y. Kim, "STM-induced luminescence from single phthalocyanine molecules", 12th International Conference on Atomically Controlled Srufaces, Interfaces and Nanostructures (ACSIN-12), Tsukuba, Japan (Nov. 2013).

10. E. Minamitani, Y. Fu, Q. Xue, and Y. Kim, "Adsorption induced spin-state change in MnPc/Pb(111)", 12th International Conference on Atomically Controlled Srufaces, Interfaces and Nanostructures (ACSIN-12), Tsukuba, Japan (Nov. 2013).

11. C.-L. Lin, R. Arafune, K. Kawahara, M. Kanno, N. Tsukahara, E. Minamitani, Y. Kim, M. Kawai, and N. Takagi, "The electronic structure of single layer silicene on Ag(111)", 12th International Conference on Atomically Controlled Srufaces, Interfaces and Nanostructures (ACSIN-12), Tsukuba, Japan (Nov. 2013).

12. T. K. Shimizu, J. Jung, H. Imada, and Y. Kim, "STM study of photochromic diarylethene adsorbed on noble metals", 12th International Conference on Atomically Controlled Srufaces, Interfaces and Nanostructures (ACSIN-12), Tsukuba, Japan (Nov. 2013).

13. R. Arafune, C.-L. Lin, K. Kawahara, M. Kanno, N. Tsukahara, E. Minamitani, Y. Kim, M. Kawai, and N. Takagi, "Geometric and electronic structure change of silicene by interacting with Ag(111): DFT analysis", 12th International Conference on Atomically Controlled Srufaces, Interfaces and Nanostructures (ACSIN-12), Tsukuba, Japan (Nov. 2013).

14. Y. Kim, "Single molecule chemistry", 3rd Asia-Korea Conference on Science and Technology 2013 (AKC 2013), Singapore, (Nov. 2013).

15. Y. Kim, "Electronic property control of 2-D molecular systems", 2013 International Symposium on Additive Manufacturing and Printed Electronics, Jeju, Korea, (Nov. 2013). (Invited)

16. J. Jung, H.-J. Shin, M. Kawai, and Y. Kim, "Controlling surface reactivity of ultrathin insulating film by interface manipulation", IBS-RIKEN mini-Workshop on Surface Science, Daejeon, Korea, (Feb. 2014).

17. Y. Kim, "Energetics of nanoscale molecular interfaces", 2014 Korea-Japan Joint International Symposium on Molecular Systems (KJMS 2014), Muju, Korea, (Feb. 2014).

18. H. Imada, H. Imai, M. Kawai, and Y. Kim, "STM-induced luminescence from single phthalocyanine molecules", 2014 Korea-Japan Joint International Symposium on Molecular Systems (KJMS 2014), Muju, Korea, (Feb. 2014).

19. Y. Kim, "STM investigation of interactions in self-assembled organic monolayers", 247th ACS (American Chemical Society) National Meeting & Exposition, Dallas, Texas, USA, (Mar. 2014). (Invited)